Synthesis and Characterization of Amorphous Hydrated Alkali Thio-Hydroxogermanates

Steven A. Poling, Carly R. Nelson, and Steve W. Martin*

Department of Materials Science and Engineering, 2220 Hoover Hall, Iowa State University of Science and Technology, Ames, Iowa 50011

Received July 13, 2004. Revised Manuscript Received January 24, 2005

The synthesis, structure, and nonhumidified proton conductivity of the hydrated alkali thio-hydroxogermanates, denoted as $M_xGeS_x(OH)_{4-x}{\cdot}yH_2O$ ($1 \le x \le 4$, $0 < y < 8$) for M = Na, K, Rb, and Cs, are reported. These materials are generally X-ray amorphous when produced by a low-temperature (∼75 °C) aqueous solution evaporation−precipitation route. Raman and IR spectroscopies indicate mixed chalcogenide germanium central anions with distinct asymmetric Ge−O and symmetric Ge−S stretching modes observable around 820−754 and 500−325 cm^{-1}, respectively. These thio-oxoanions possess a combination of thermally stable hydroxyl groups and hydrophilic alkali associated with the nonbridging sulfurs. Alternating current impendence measurements performed under anhydrous conditions on low-pressure sealed pellets reveal fast ionic conductivity, 10^{-3}−10^{-2} S/cm, for typical temperatures between 100 and 275 °C. The observed falloff in conductivity at higher temperatures is consistent with the appearance of endothermic transitions in differential scanning calorimetry measurements of hermetically sealed samples, presumably from the "boiling" or sublimation of a crystalline water sublattice. Corresponding onset temperatures were observed between 150 and 275 °C and dependent on the alkali and composition. Under dry atmosphere conditions, thermogravimetric analysis mass loss measurements indicate continuous mass loss above the preparation temperature of ∼75 °C.

Introduction

The emergence of H_2−O_2 fuel cells as an alternative energy source for portable applications is driven by the possibility of using renewable hydrogen fuels coupled with high efficiencies and low green house gas emissions. Central to the operation of the proton-based fuel cell is the proton exchange membrane (PEM) transporting protons from the anode to the cathode while providing electronic insulation. Normally, the PEM is a hydrated perfluorinated polymer, such as Nafion, that contains a small proportion of sulfonic or carboxylic ionic functional groups. These classes of hydrated polymers are generally expensive and restricted by strong humidification requirements to operating temperatures below 100 °C. To obtain higher efficiencies and easier water (steam) management, intermediate temperature ($100 < T <$ 300 °C) proton-conducting materials must be developed for the PEM.

Much recent effort has been expended to develop organic,[1−3] inorganic,[4−10] and organic−inorganic proton-conducting materials[11−14] for use in the intermediate temperature range. Generally inorganic networks possess better thermal stability yet are limited in application by solubility, dehydration, phase transitions, and/or melting at elevated temperatures. For example, many anhydrous hydroxide compounds without notable hydrogen bonding, such as the alkali hydroxides,[15] are reasonably thermally stable and ionic in nature but often melt or never have acceptable proton conductivities before thermally decomposing. In contrast, many hydrated compounds typically exhibit medium to weak hydrogen bonding and fast proton conductivity but thermally decompose at elevated temperatures with the loss of water. The "boiling" or sublimation of the hydrated water associated with the thermal decomposition generally occurs for temperatures less than ∼400 °C.[5,8,10,17,18] Ideally, high relative humidity (RH) atmospheres may be used to compensate for any dehydration

* To whom correspondence should be addressed. E-mail: swmartin@iastate.edu. Fax: (515) 294-5444.

(1) Bae, J.-M.; Honma, I.; Murata, M.; Yamamoto, T.; Rikukawa, M.; Ogata, N. *Solid State Ionics* **2002**, *147*, 189−194.
(2) Alberti, G.; Casciola, M. *Solid State Ionics* **2001**, *145*, 3−16.
(3) Colomban, Ph. *Ann. Chim. Sci. Mater.* **1999**, *24*, 1−18.
(4) Tsuru, T.; Yagi, Y.; Kinoshita, Y.; Asada, M. *Solid State Ionics* **2003**, *158*, 343−350.
(5) Hara, S.; Sakamoto, H.; Miyayama, M.; Kudo, T. *Solid State Ionics* **2002**, *154*−*155*, 679−685.
(6) Matsui, T.; Takeshita, S.; Iriyama, Y.; Abe, T.; Inaba, M.; Ogumi, Z. *Electrochem. Commun.* **2004**, *6*, 180−182.
(7) Tanaka, Y.; Matsuda, H.; Hibino, M.; Kudo, T. *Trans. Mater. Res. Soc. Jpn.* **2001**, *26*, 1075−1078.
(8) Li, Y. M.; Hibino, M.; Miyayania, M.; Kudo, T. *Solid State Ionics* **2000**, *134*, 271−279.
(9) Haile, S. M.; Boysen, D. A.; Chisholm, C. R. I.; Merle, R. B. *Nature* **2001**, *410*, 910−913.
(10) Ozawa, K.; Wang, J.; Ye, J.; Sakka, Y. *Chem. Mater.* **2003**, *15*, 928−934.
(11) Kumar, B.; Fellner, J. P. *J. Power Sources* **2003**, *123*, 132−136.
(12) Honma, I.; Nakajima, H.; Nomura, S. *Solid State Ionics* **2002**, *154*−*155*, 707−712.
(13) Honma, I.; Nakajima, H.; Nishikawa, O.; Sugimoto, T.; Nomura, S. *Solid State Ionics* **2003**, *162*−*163*, 237−245.
(14) Nakajima, H.; Honma, I. *Solid State Ionics* **2002**, *148*, 607−610.
(15) Spaeth, M.; Kreuer, K. D.; Dippel, Th.; Maier, J. *Solid State Ionics* **1997**, *97*, 291−297.
(16) Spaeth, M.; Kreuer, K. D.; Maier, J. *J. Solid State Chem.* **1999**, *148*, 169−177.
(17) Mikuli, E.; Migdal-Mikuli, A.; Chyzy, R.; Grad, B.; Dziembaj, R. *Thermochim. Acta* **2001**, *370*, 65−71.
(18) Stoilova, D.; Koleva, V. *Thermochim. Acta* **1996**, *290*, 85−91.

10.1021/cm0488581 CCC: $30.25
Published on Web 03/09/2005

for temperatures below this transition. Thus an inorganic hydrate with an elevated steam point and reversible hydration behavior would be well suited as an intermediate temperature proton conductor.

Because of the ionic and hydrophilic nature of the alkali species, salts and alkali hydroxides are generally easily hydrated and reasonably thermally stable. Additionally, the sulfides are more covalent in nature than the oxides with the greater polarizability of sulfur producing weaker Coulombic or electrostatic interactions with mobile ions. However, sulfides tend to be chemically reactive with water. These general observations have motivated a search for a mixed oxygen−sulfide (oxy-sulfide) anion that may be a reasonable compromise for proton conductivity, chemical stability, and solubility. Previously, an open framework mixed oxy-sulfide framework was isolated in the form of the fully hydrated crystalline sodium thio-hydroxogermanates.[19,20] These highly soluble crystalline products were precipitated by drying from acetone and water solutions, where the acetone-to-water ratios were greater than 2 and typically 3−5, at room temperature; reactants included NaOH, Na_2S, GeO_2, and/or GeS_2.[19,20] An orthorhombic unit cell with space group *Pbcn* was reported for $Na_2GeS_2(OH)_2 \cdot 5H_2O$,[19,20] and a monoclinic unit cell with space group *C*2/*c* was reported for $Na_3GeS_3(OH) \cdot 8H_2O$.[20] Structurally, very basic oxygens, with *d*(Ge−O) of 1.812 and 1.877 Å for the di- and trivalent thio-hydroxogermanate ions, respectively, were observed; this compares to normal germanates with *d*(Ge−O) ranging between 1.71 and 1.78 Å.[19,20] The weaker ionic bonding associated with Ge−OH units suggests delocalization of the electrons on Ge by the covalently bonded Ge−S units. Additionally, extensive hydrogen bonding was observed with S···HO and O···HO connecting the thio-oxoanions to the alkali.

In our work, the fully hydrated crystalline sodium thio-hydroxogermanates proved to be difficult to isolate and too fragile. Previously, we reported a new class of amorphous hydrated mixed anion alkali thio-hydroxogermanates for potential application as intermediate temperature proton conductors.[21] On the basis of the starting reactants, reaction product masses, and vibrational spectroscopy, the Cs-based amorphous material was written as $Cs_2GeS_2(OH)_2 \cdot yH_2O$. Additionally, this new material was demonstrated to have fast proton conductivity and increased thermal stability against dehydration even at low RH levels, 0−10%. Here we expand the alkali modification to include other alkali (Na, K, and Rb) and different reactant ratios of alkali hydrosulfide (MSH) to germanium oxide (GeO_2). The amorphous structure and proton conductivity mechanism are discussed from these modifications.

Experimental Section

Sample Preparation. Attempts to synthesize hydrated materials of the general form $M_xGeS_x(OH)_{4-x} \cdot yH_2O$ ($1 \le x \le 4$; $0 < y < 8$) for M = Na, K, Rb, and Cs were performed using aqueous solutions containing stoichiometric amounts of the alkali hydrosulfide, MSH prepared by room-temperature reactions of excess liquid H_2S with the corresponding alkali hydroxide followed by draining off the excess H_2S (patent pending,[22] 97.9−99.9%), and commercial quartz-type GeO_2 (Cerac 99.999%, ∼325 mesh). Ideally, the corresponding reactions may be written as

$$x\mathrm{MSH} + \mathrm{GeO_2} + (y + 2 - x)\mathrm{H_2O} \rightarrow \mathrm{M}_x\mathrm{GeS}_x(\mathrm{OH})_{4-x} \cdot y\mathrm{H_2O},\ 1 \le x \le 4 \quad (1)$$

Best results were obtained by dissolving 0.5 g batches of the reactants in 5 mL of deionized H_2O supersaturated by stirring and heating at ∼75 °C. A dried translucent film was deposited after allowing the excess water to evaporate at ∼75 °C for one week. The samples were then stored under a dry He atmosphere where careful mass measurements and preparations for sample characterizations were performed. Note that similar reaction products may be produced using other reactants including MOH, M_2O, M_2S, and GeS_2.

Structural Characterization. Structural investigations were performed using IR absorption, Raman scattering, and powder X-ray diffraction (XRD). The IR absorption spectra were collected at 298 K with a Bruker IFS 66v/S spectrometer using 32 scans and 4-cm^{-1} resolution in both the mid- and far-IR regions. Translucent CsI pellets were prepared for transmission by mixing in ∼1 wt. % of powder sample and pressing. The Raman scattering spectra were collected at 298 K with a Bruker FT-Raman RFS 100/S spectrometer using a 1064-nm Nd:YAG laser, 32 scans, 2-cm^{-1} resolution, and 300 mW of power focused on ∼0.1-mm diameter spot size. Powdered samples were packed into a small aluminum cuplike sample holder and covered with a clear amorphous tape. Powder XRD spectra were collected at 298 K with a Scintag XDS-2000 diffractometer using Cu Kα radiation (λ = 1.541 78 Å), 40 kV, and 30 mA. Scans were performed between 20 to 120° 2θ using a 0.02° step size and 0.5-s dwell time. Powdered samples were packed into a recessed square polycarbonate sample holder and covered with 0.025 mm thick Kapton (Polyimide) tape to seal out atmospheric moisture and oxygen.

Thermal Characterization. Phase transitions were investigated using a Perkin-Elmer diamond differential scanning calorimeter. About 15 mg of sample was placed in a volatile aluminum sample pan and hermetically sealed. The sample was then heated at a rate of 10 °C/min from 50 to 300 °C. Thermal mass loss measurements were performed with a Perkin-Elmer Thermogravimetric Analyzer TGA 7 (TGA). About 4 mg of sample was placed in an open aluminum sample pan. The sample was then heated at a rate of 10 °C/min from 50 to 500 °C using a 20 mL/min flow of N_2 as the sample purge gas.

Conductivity Measurements. Alternating current (AC) impedance data were collected with a Gamry PC4/750 potentiostat in the frequency range of 0.2 to 100 kHz using 0.5-V amplitude on compacted powder samples. Hardened steel blocking electrodes with a 6.35-mm outside diameter were pressed inside an undersized Teflon sleeve containing ∼100 mg of sample. A pressure of ∼562 MPa was applied to produce an average pellet thickness of ∼0.5 mm. Constant pressure was maintained on the pellet during the measurement by the electrodes and an aluminum "O" frame insulated from the electrodes with Teflon. The pellet/electrode/frame assembly was contained inside a silica cell that maintained 1 atm pressure of He above the sample. The bottom of the cell was placed into a custom-built crucible furnace and data were collected using increments of 10−15 °C after allowing the sample temperature to stabilize to within ±0.5 °C before the next data set was collected,

(19) Krebs, B.; Wallstab, H. *Z. Naturforsch.* **1981**, *36b*, 1400−1406.
(20) Krebs, B.; Wallstab, H. *Inorg. Chim. Acta* **1981**, *54* L123-L124.
(21) Poling, S. A.; Nelson, C. R.; Martin, S. W. **2004**, submitted.
(22) Martin, S. W.; Poling, S. A.; Sutherland, J. T. U.S. Patent 10,627,-584, **2003**.

Table 1. Reactants, Proposed Reaction Products, and Corresponding Endothermic Onset Temperatures for the Amorphous Alkali Thio-Hydroxogermanates (Onset Temperature Error Is from Multiple Samples)

reactants ($+n$$H_2O$)	dry reactant mass (g)	dry product mass (g)	*proposed product* ($\cdot y$$H_2O$)	*y*	DSC endo onset (°C)
$CsSH + GeO_2$	0.500	~0.499	$CsGeS(OH)_3$	< 0	~275
$2NaSH + GeO_2$	0.500	~0.555	$Na_2GeS_2(OH)_2$	~1.3	179 ± 3
$2KSH + GeO_2$	0.500	0.515−0.527	$K_2GeS_2(OH)_2$	0.4−0.8	235 ± 3
$2RbSH + GeO_2$	0.500	~0.522	$Rb_2GeS_2(OH)_2$	~0.8	~232
$2CsSH + GeO_2$	0.500	0.505−0.512	$Cs_2GeS_2(OH)_2$	0.2−0.6	264 ± 6
$3NaSH + GeO_2$	0.500	0.591−0.612	$Na_3GeS_3(OH)$	3.8−4.4	~212
$3KSH + GeO_2$	0.500	0.528−0.534	$K_3GeS_3(OH)$	2.0−2.2	236 ± 2
$3RbSH + GeO_2$	0.500	0.522−0.534	$Rb_3GeS_3(OH)$	2.2−2.6	219 ± 2
$3CsSH + GeO_2$	0.500	0.512−0.534	$Cs_3GeS_3(OH)$	1.8−3.2	239 ± 10
$4CsSH + GeO_2$	0.500	0.529−0.531	Cs_4GeS_4	4.5−4.7	250 ± 9

Table 2. Suggested Vibrational Mode Assignments for the As-Prepared Amorphous Alkali Thio-hydroxogermanates[a]

vibrational mode	$CsSH + GeO_2 + nH_2O$	$2MSH + GeO_2 + nH_2O$	$3MSH + GeO_2 + nH_2O$	$4CsSH + GeO_2 + nH_2O$	$Na_2GeS_2(OH)_2 \cdot 5H_2O$[19,20]	$Na_3GeS_3(OH) \cdot 8H_2O$[19,20]
$\upsilon_s(Ge-S^-)$: ortho-			336−328 Raman	~327 Raman		
pyro-			389−385 Raman	~387 Raman		385
meta-		421−404 IR, Raman	420−418 Raman	~418 Raman	415 Raman	
di-	~460 IR, Raman; ~503, ~476 Raman		456−450 Raman	~451 Raman		
$\upsilon_{as}(Ge-S^-)$: pyro-			417−403 IR	~408 IR		417
meta-		454−449 IR, Raman	457−448 IR, Raman	451−449 IR, Raman	454 IR, Raman	
di-	~548 IR					
$\upsilon_s(Ge-OH)$	664−662 IR, Raman	627−614 IR, Raman	630−611 IR, Raman		618 Raman	
$\upsilon_{as}(Ge-OH)$	~754 IR	781−762 IR	777−770 IR	~781 IR	765 IR	
$(Ge-O^-)$	820−809 IR					
$R(H_2O)$ and $R(OH^-)$			457−448 IR, Raman	451−449 IR, Raman		
			542−530 IR, Raman	534−531 IR, Raman		
		668−660 IR, Raman	677−658 IR, Raman	659−658 IR, Raman		
		~881 IR	881−879 IR	~879 IR		
	~995 IR	1007−995 IR, Raman	1007−987 IR, Raman	~987 IR, Raman		
	~1113 IR	1151−1134 IR	1146−1128 IR, Raman	1132−1111 IR, Raman		
		1391−1365 IR	1396−1375 IR	~1373 IR		
	~1450 IR	1446−1431 IR	1446−1427 IR	~1441 IR		
$\delta(H-O-H)$	~1649 IR	1666−1635 IR	1668−1630 IR	~1651 IR		
$\upsilon(S\cdots H_2O)$		2147−2136 IR	2160−2137 IR			
$\upsilon(O-H)$	~3360 IR	3371−3333 IR	3416−3331 IR	~3371 IR		

[a] Assignments from the literature for the germanium sulfide and germanium oxide units in the crystalline sodium thio-hydroxogermanates are also presented,[19,20] although modes for the OH^- and H_2O units were not given. All units are in wavenumbers (cm^{-1}).

typically requiring no more than 30 min. Typically two heating runs were conducted on every sample. During the first run, the conductivity data were collected on heating for the first time. For the second run, the data were collected on heating after the sample had been previously cooled back to room temperature. During all of these measurements the sample cell was not opened and the atmosphere remained pure He. The direct current (DC) conductivity values were determined from the intersection of the observed depressed semicircle and the low-frequency polarization "tale" in the Nyquist plot of the complex impendence.

Results and Discussion

Sample Preparation. The stable form of the amorphous alkali thio-hydroxogermanates (i.e., liquidlike gel vs solid) is a function of temperature and RH. At room temperature, these materials behave very similarly to alkali salts with respect to solubility in water, i.e., water readily hydrates the component alkali. Under dry or noncondensing conditions above the steam point, these materials are mechanically robust and easily powdered and pressed into membranes. Table 1 presents a list of reactants and proposed reaction products after one week of drying time at ~75 °C. During the drying process, slightly different time, temperature, and/or RH conditions produced slightly different reaction product masses. From vibrational spectroscopy, these mass differences are attributed to the amount of intercalated water. As is apparent from mass measurements, the $CsSH + GeO_2 + nH_2O$ reaction did not produce a pure hypothetical phase of $CsGeS(OH)_3$. In contrast, $2MSH + GeO_2 + nH_2O$ reaction product masses are consistent with $M_2GeS_2(OH)_2 \cdot yH_2O$, where $0.2 < y < 1.3$. The $3MSH + GeO_2 + nH_2O$ reaction product masses are consistent with $M_3GeS_3(OH) \cdot yH_2O$, where $1.8 < y < 4.4$. Finally, the $4CsSH + GeO_2 + nH_2O$ reaction product masses are consistent with $Cs_4GeS_4 \cdot yH_2O$, where $4.5 < y < 4.7$. As expected, the water content is correlated to the amount of alkali and consistent with a hydrated cation shell. Interestingly, the Na phases appear to have the largest quantity of hydrated water.

Structural Characterization: XRD. Powder X-ray diffraction patterns indicate the as-prepared alkali thio-hydroxogermanates are noncrystalline. Figure 1 presents the powder diffractograms for the $xCsSH + GeO_2 + nH_2O$ reaction products ($x = 2$ and 4) using a Polyimide tape cover to prevent hydration at ambient conditions; no diffraction peaks are observed distinguishable from the background between 20 to 120° 2θ. The X-ray amorphous nature of the reaction products is consistent with the evaporation−precipitation preparation route employed at ~75 °C, and no evidence is observed for the presence of the crystalline reactants, i.e., MSH and quartz-type GeO_2. In comparison, excessive amounts of acetone were used at room temperature to isolate the crystalline $Na_2GeS_2(OH)_2 \cdot 5H_2O$[19,20] and $Na_3GeS_3(OH) \cdot 8H_2O$[20] phases from solution. Crystalline products are also

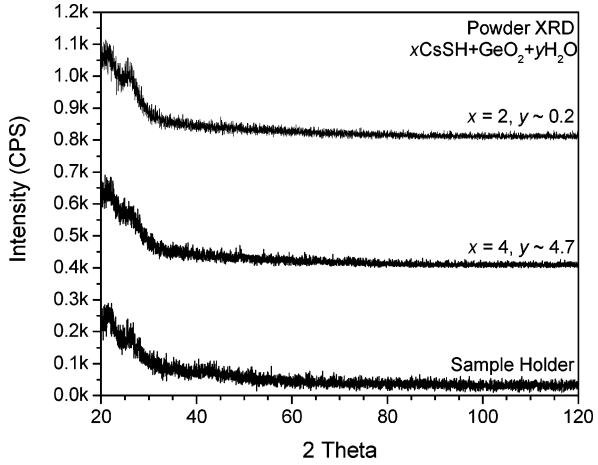

Figure 1. Powder XRD diffractograms for the as-prepared xCsSH + GeO_2 + $n$$H_2O$ reaction products (x = 2 and 4). Scans were obtained from finely powdered samples covered with 0.001 in. thick Kapton (Polyimide) tape. An empty polycarbonate sample holder covered with tape is shown as a reference.

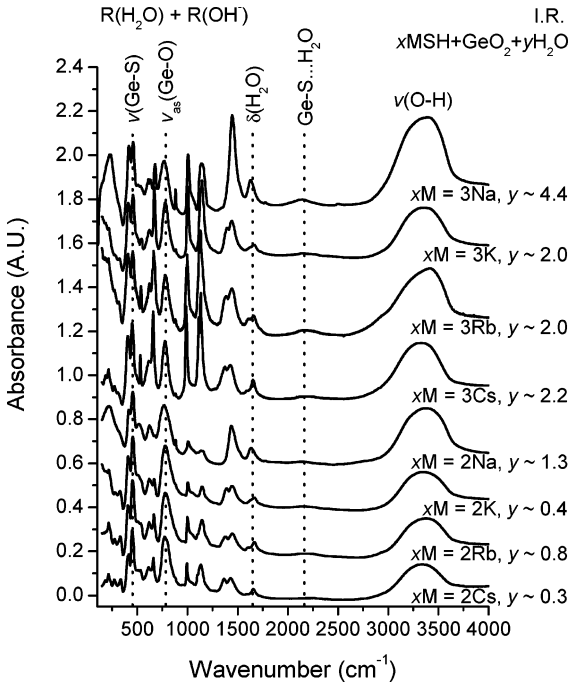

Figure 2. IR absorption spectra for the as-prepared xMSH + GeO_2 + $n$$H_2O$ reaction products (x = 2 and 3; M = Na, K, Rb, and Cs). Vibrational modes attributable to Ge-S^-, Ge−O^-, and O−H bond stretching are observed with peak intensities between 457 and 403, 783−761, and 3413−3330 cm^{-1}, respectively. Additionally, H_2O and O−H rotatory (librations) modes are generally observed as sharp bands between 1446 and 534 cm^{-1}.

reported from solid-state reactions for Li_4GeS_4[23] and Na_4GeS_4[24] phases.

Structural Characterizations: IR. The IR spectra indicate the presence of mixed chalcogenide complex anions with a central Ge atom and hydrated water. Figure 2 presents the IR spectra for the as-prepared xMSH + GeO_2 + $n$$H_2O$ reaction products (x = 2 and 3; M = Na, K, Rb, and Cs), Figure 3 presents the IR spectra for the as-prepared xCsSH + GeO_2 + $n$$H_2O$ reaction products (x = 1, 2, 3, and 4), and Figure 4 presents the IR spectra of the 2CsSH + GeO_2 + $n$$H_2O$ reaction products after performing AC impedance measurements using dry or humidified air at a fixed temperature.[21] In each spectrum, strong vibrational bands observable between 820 and 754 cm^{-1} may be attributed to the asymmetric terminal Ge−O^- stretching mode. This mode is typically observed between 1000 and 700 cm^{-1} for low alkali modified germanate glasses[25] and reported at 765 cm^{-1} for $Na_2GeS_2(OH)_2 \cdot 5H_2O$.[19] Individual peaks are observed between 781 and 762 cm^{-1} for the 2MSH + GeO_2 + $n$$H_2O$, 3MSH + GeO_2 + $n$$H_2O$, and 4CsSH + GeO_2 + $n$$H_2O$ reaction products. In contrast, two overlapping peaks are observed at 820 and 754 cm^{-1} for the CsSH + GeO_2 + $n$$H_2O$ reaction product (see Figure 3). The appearance of a second

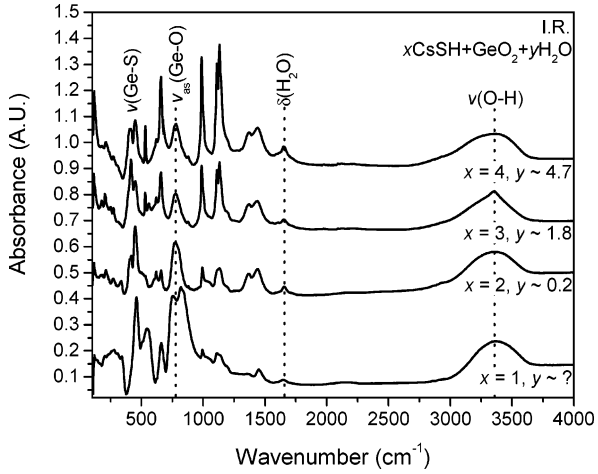

Figure 3. IR absorption spectra for the as-prepared xCsSH + GeO_2 + $n$$H_2O$ reaction products (x = 1, 2, 3, and 4). Vibrational modes attributable to Ge-S^-, Ge−O^-, and O−H bond stretching are generally observed with peak intensities between 459 and 407, 819−754, and 3371−3353 cm^{-1}, respectively. Additionally, H_2O and O−H rotatory (librations) modes are generally observed as sharp bands between 1450 and 531 cm^{-1}.

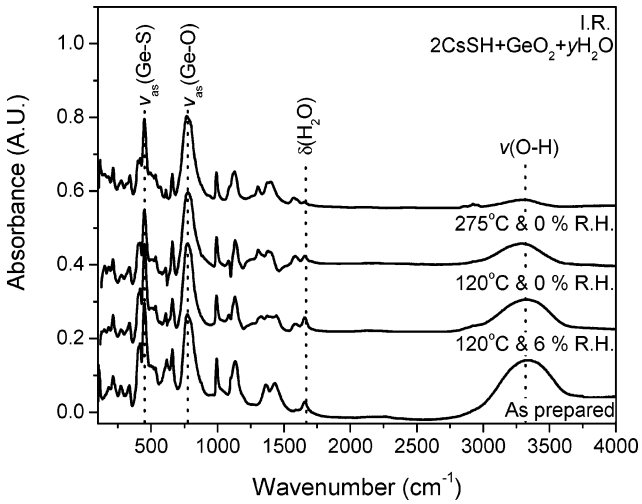

Figure 4. IR absorption spectra of the 2CsSH + GeO_2 + $n$$H_2O$ reaction products after performing AC impedance measurements using dry or humidified air at a fixed temperature.[21] The vibrational band intensities attributable to molecular H_2O and O−H groups are reduced with increasing temperature and decreasing RH. In contrast, vibrational modes attributable to structural Ge−S^- and Ge−O^- stretching are unchanged with dry air and temperatures as high as 275 °C.

(23) Matsushita, Y.; Kanatzidis, M. G. *Z. Naturforsch., B: Chem. Sci.* **1998**, *53*, 23−30.
(24) Olivier-Fourcade, J.; Ribes, M.; Philippot, E.; Maurin, M. *Comptes Rendus des Seances de l'Academie des Sciences, Serie C: Sciences Chimiques* **1971**, *272*, 1964−1967.
(25) Efimov, A. M. *Phys. Chem. Glasses* **1999**, *40*, 199−206.

higher frequency peak between 830 and 820 cm^{-1} is usually associated with a terminal $Ge-O^-$ (M^+) stretching mode.[25] Strong vibrational bands between 548 and 403 cm^{-1} may be generally attributed to symmetric and asymmetric terminal $Ge-S^-$ stretching modes. Generally, these modes decrease in frequency with increasing alkali modifier content; this behavior is consistent with an increase in the reduced vibrational mass due to nonbridging sulfurs.

Water bands attributable to O−H stretching and H−O−H bending are observed with peak intensities between 3416 and 3331 and 1630−1668 cm^{-1}, respectively. The broad vibrational band centered around 2160−2136 cm^{-1} may be attributed to hydrogen bonding of the hydrated water to terminal sulfurs, i.e., $Ge-S^-\cdots H_2O$. Additionally, there are eight sharp vibrational bands between 1450 and 448 cm^{-1} that are observed to decrease in intensity (from ∼0.2 to 0.05 absorbance units as shown in Figure 4) with dehydration; generally, these bands may be attributed to rotatory (librations) modes of hydroxide ions and/or water molecules. After they were subjected to a temperature of 275 °C and 0% RH, these bands are observed to decrease in the IR spectra of the $2CsSH + GeO_2 + nH_2O$ reaction product (see Figure 4), whereas vibrational bands attributable to terminal $Ge-S^-$ and $Ge-O^-$ stretching modes remain unaffected. Normally rotary modes occur between 300 and 800 cm^{-1} but have been reported as high as 1050 cm^{-1}.[26] The higher-frequency 1440 and 1375 cm^{-1} bands may also be attributed to M_2CO_3 contamination from the starting alkali hydrosulfide reactants; a doublet is reported between 1450−1410 cm^{-1} for υ_3 asymmetric stretching of the CO_3^{2-} unit for Li_2CO_3.[27] However, the remaining vibrational modes associated with the CO_3^{2-} unit, namely, υ_1 symmetric stretching at 1065 cm^{-1} (Raman), υ_2 out-of-plane bending at 880−850 cm^{-1} (IR), and υ_4 in-plane bending at 720−680 cm^{-1} (IR, Raman), are not observable in the corresponding IR or Raman spectra. Additionally, no other contaminants are observed in the vibrational spectra including those of the starting MSH and quartz-type GeO_2 reactants as would be observed by a strong S−H stretching mode between 2508 and 2556 cm^{-1} (IR, Raman)[28,29] and asymmetric and symmetric Ge−O stretching modes between 989 and 860 cm^{-1} (IR) and 569−464 cm^{-1} (IR, Raman),[25] respectively.

Structural Characterizations: Raman. The corresponding Raman spectra for the as-prepared alkali thio-hydroxo-germanates also suggest the presence of mixed oxy-sulfide anions. Figure 5 presents the Raman spectra for the as-prepared $xMSH + GeO_2 + nH_2O$ reaction products ($x = 2$ and 3; M = Na, K, Rb, and Cs), and Figure 6 presents the Raman spectra for the as-prepared $xCsSH + GeO_2 + nH_2O$ reaction products ($x = 1$, 2, 3, and 4). The Raman spectrum of the $CsSH + GeO_2 + nH_2O$ reaction product (see Figure 6) exhibits three specific vibrational bands with peak intensities between 503 and 406 cm^{-1} that may be attributed to stretching modes of terminal $Ge-S^-$ modes, of bridging Ge−O−Ge units, and of nonbridging $Ge-O^-$ (H+) and $Ge-O^-$ (M^+) units. Additionally, a coordination of four is assumed for Ge in these amorphous alkali thio-hydroxo-germanates, because there does not exist any vibrational spectrographic evidence in the literature to differentiate between the existence of Ge^{4+} (tetrahedral coordination) vs Ge^{6+} (octahedral coordination).[25] For pure sulfides, germanium appears only as Ge^{4+}, whereas in pure oxides Ge^{6+} can be manifest with alkali modification. More work is

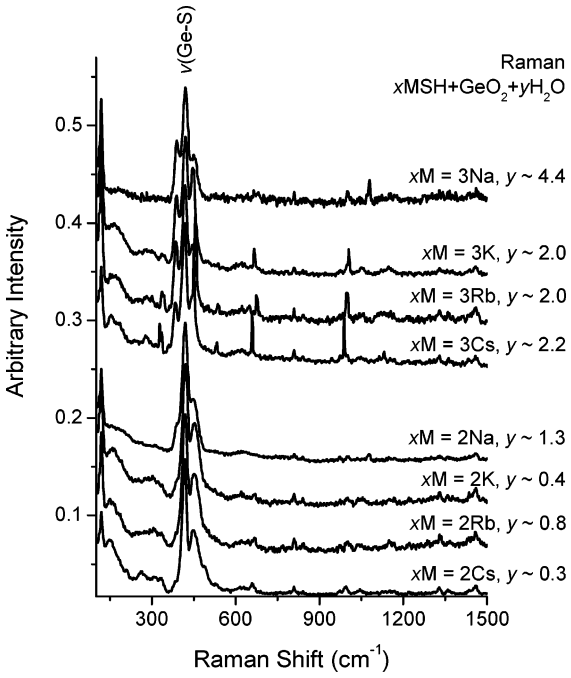

Figure 5. Raman scattering spectra for the as-prepared $xMSH + GeO_2 + nH_2O$ reaction products ($x = 2$ and 3; M = Na, K, Rb, and Cs). Vibrational modes attributable to $Ge-S^-$ bond stretching are observed with peak intensities between 385 and 456 cm^{-1}. Sharp vibrational bands appearing at and above ∼450 cm^{-1} may be attributed to H_2O and O−H rotatory (librations) modes.

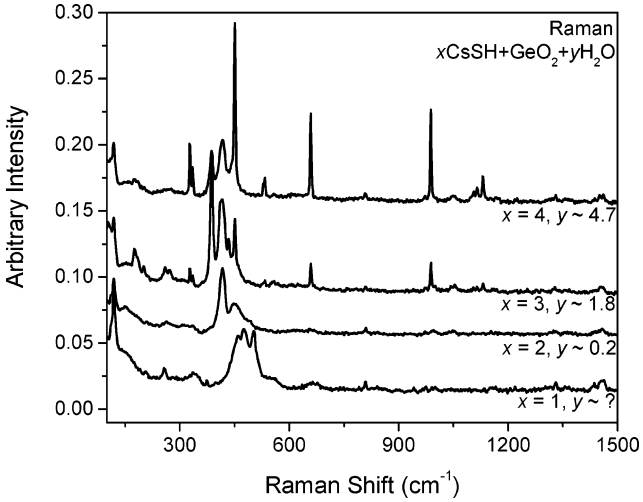

Figure 6. Raman scattering spectra for the as-prepared $xCsSH + GeO_2 + nH_2O$ reaction products ($x = 1$, 2, 3, and 4). Vibrational modes attributable to $Ge-S^-$ bond stretching are generally observed with peak intensities between 502 and 327 cm^{-1}. Sharp vibrational bands appearing at and above ∼450 cm^{-1} may be attributed to H_2O and O−H rotatory (librations) modes.

(26) Lutz, H. D.; Eckers, W.; Schneider, G.; Haeuseler, H. *Spectrochim. Acta* **1981**, *37A*, 561−567.
(27) Pasierb, P.; Komornicki, S.; Rokita, M.; Rekas, M. *J. Mol. Struct.* **2001**, *596*, 151−156.
(28) Beckenkamp, K.; Lutz, H. D.; Jacobs, H.; Metzner, U. *J. Solid State Chem.* **1994**, *109*, 241−250.
(29) Lutz, H. D.; Beckenkamp, K.; Jacobs, H.; Kirchgassner, R. *J. Raman Spectrosc.* **1994**, *25*, 395−402.

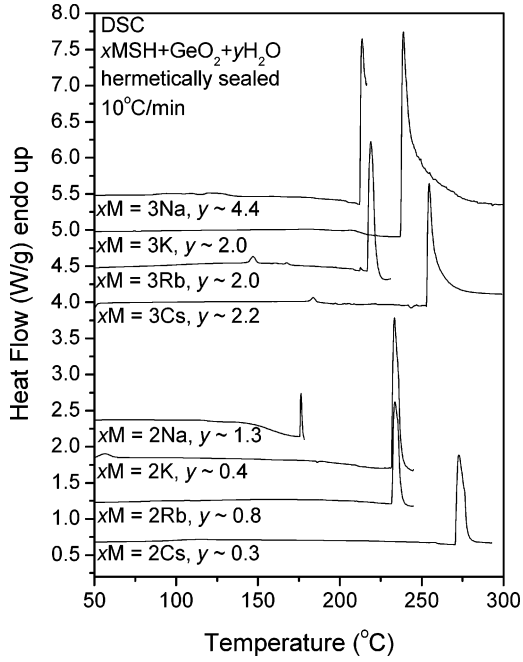

Figure 7. DSC thermograms for the as-prepared xMSH + GeO_2 + $n H_2O$ reaction products (x = 2 and 3; M = Na, K, Rb, and Cs). Samples were hermetically sealed in aluminum pans, heated at 10 °C/min, and purged with N_2. For some samples, additional endothermic peaks were also recorded at slightly higher temperatures (not shown). The strong endothermic peaks observed between 176 and 275 °C suggest a crystalline water sublattice.

needed here to more clearly clarify the coordination of the germanium center.

The Raman spectra of the 2MSH + GeO_2 + $n H_2O$ reaction products suggest the unique presence of $GeS_2O_2^{4-}$ ions with asymmetric and symmetric terminal Ge−S^- stretching modes observable between 454 and 449 and 421−404 cm^{-1}, respectively. A similar thio-oxoanion of approximate C_{2v} point symmetry group was previously reported for $Na_2GeS_2(OH)_2 \cdot 5H_2O$ with $\upsilon_6(B_1)$ asymmetric and $\upsilon_1(A_1)$ symmetric terminal Ge−S^- stretching modes observable at ∼454 and 415 cm^{-1}, respectively.[19] In contrast, the 3MSH + GeO_2 + $n H_2O$ and 4CsSH + GeO_2 + $n H_2O$ reaction products exhibit more vibrational disorder. Their corresponding spectra show evidence of GeS_4^{4-}, GeS_3O^{4-}, $GeS_2O_2^{4-}$, and $GeSO_3^{4-}$ ions with symmetric terminal Ge−S^- stretching modes assigned at 336−327, 389−385, 420−418, and 456−450 cm^{-1}, respectively. These values illustrate the same general trend in frequency as those previously reported for sodium pyrothiogermanate $Na_6Ge_2S_7$ (380−450 cm^{-1}), sodium metathiogermanate Na_2GeS_3 (370−450 cm^{-1}), and sodium dithiogermanate $Na_4Ge_4S_{10}$ (470 cm^{-1}).[30] A GeS_3O^{4-} thio-oxoanion of approximate C_{3v} point symmetry group was also previously reported for $Na_3GeS_3(OH) \cdot 8H_2O$[20] with asymmetric and symmetric terminal Ge−S^- stretching modes observable at ∼417 and 385 cm^{-1}, respectively.

Thermal Characterizations: DSC. Figure 7 presents the DSC thermograms for the as-prepared xMSH + GeO_2 + $n H_2O$ reaction products (x = 2 and 3; M = Na, K, Rb, and Cs), Figure 8 presents the DSC thermograms for the as-prepared xCsSH + GeO_2 + $n H_2O$ reaction products (x = 1, 2, 3, and 4), and Table 1 lists the corresponding endothermic peak onset temperatures. Typically, only one strong endothermic transition is observed in the temperature range of 175−275 °C for each amorphous alkali thio-hydroxogermanate using a hermetically sealed sample pan. However, the sodium thio-hydroxogermanates were observed to exhibit multiple consecutive transitions (note only the lowest temperature transition is shown in Figure 7). The endothermic transitions are only weakly observed using high heating rates, e.g., $R \approx 40$ °C/min, with open sample pan environments as with differential thermal analysis (DTA). These transitions may be attributed to the presence of a crystalline water sublattice and the corresponding suppression of the "boiling" or sublimation point of the hydrated water by an extensive hydrogen bonded network. In this case, the volatile aluminum DSC sample pan environment ($P_{max} \approx$ 2 atm) would minimize dehydration and provide hydrated phase stability. Similar phase transitions are reported for other inorganic hydrated materials,[5,8,10,17,18] such as in the $SnO_2 \cdot nH_2O$ and $ZrO_2 \cdot nH_2O$ systems.

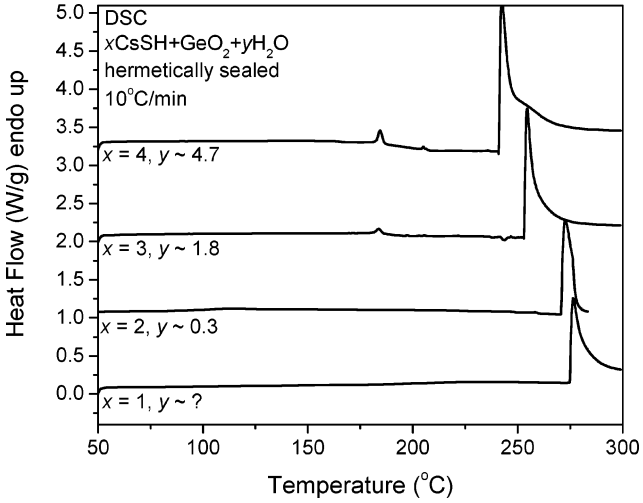

Figure 8. DSC thermograms for as-prepared xCsSH + GeO_2 + $n H_2O$ reaction products (x = 1, 2, 3 and 4). Samples were hermetically sealed in aluminum pans, heated at 10 °C/min, and purged with N_2. Higher endothermic onset temperatures, going from 240 to 275 °C, are observed with decreasing amounts of molecular H_2O.

Endothermic peak areas for the amorphous alkali thio-hydroxogermanates with a single transition typically ranged from 24 to 112 J/g or, assuming no dehydration of the sample, 4.5−32.0 kJ/mol of H_2O. These enthalpy of transition values are less than or equal to the reported enthalpy of vaporization of water in this same temperature range, i.e., 36.3 kJ/mol (180 °C) > $\Delta_{vap}H$ > 27.8 (280 °C).[31] Specific endothermic peak onset temperatures are observed between 176 and 275 °C. In the series, the cesium and sodium thio-hydroxogermanates have the highest and lowest onset temperatures, respectively. Generally, an increase in onset temperature is noted with decreasing alkali and water content as observed for the cesium thio-hydroxogermanates (see Figure 8).

(30) Barrau, B.; Ribes, M.; Maurin, M.; Kone, A.; Souquet, J. L. *J. Non-Cryst. Solids* **1980**, *37*, 1−14.

(31) *CRC Handbook of Chemistry and Physics*, 82nd ed.; Marsh, K. N., Ed.; CRC Press: New York, 2001, Sec. 6−3.

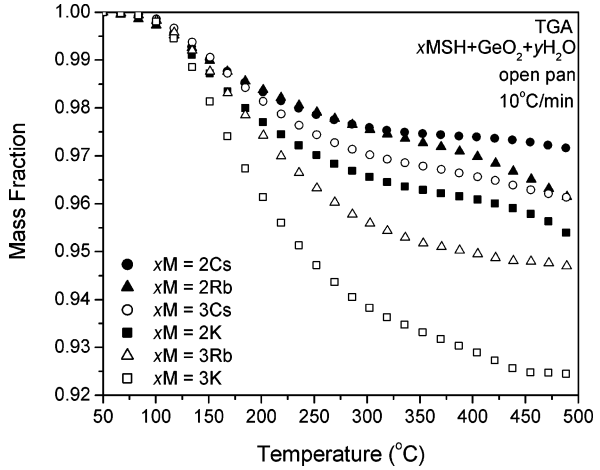

Figure 9. TGA thermograms for the as-prepared xMSH + GeO_2 + $n H_2O$ reaction products ($x = 2$ and 3; M = K, Rb, and Cs). Samples were placed in an open aluminum pan, heated at 10 °C/min, and purged with N_2. Continuous mass loss is observed above the preparation temperature of ~75 °C with a change in slope typically observable between 225 and 275 °C.

Thermal Characterizations: TGA. Continuous mass loss is observed above the preparation temperature of ~75 °C for all the alkali thio-hydroxogermanates using open sample pans purged with an atmosphere of dry N_2. Figure 9 presents the TGA thermograms for the as-prepared xMSH + GeO_2 + $n H_2O$ reaction products ($x = 2$ and 3; M = K, Rb, and Cs). Water in these hydrated materials may be generally classified in order of increasing thermal stability as chemisorbed water, water with elaborate hydrogen bonding, and structural hydroxyl groups. Chemisorbed water is typically observed to evaporate at room temperature under a dry atmosphere. In the TGA thermograms, there are generally two pronounced inflection points. From the vibrational spectra of the decomposed samples (see Figure 4) and the corresponding DSC thermograms (see Figures 7 and 8), the first inflection point at 225−275 °C may be attributed to the removal of most of the molecular water with elaborate hydrogen bonding associated with the hydrated cation shell. The second infliction point at 400−450 °C may then be attributed to the thermal decomposition of the structural hydroxyl groups and the formation of bridging oxygens.

Conductivity Measurements. AC impedance measurements reveal fast proton conductivities, i.e., $\sigma_{DC,} > 10^{-3}$ S/cm, for all the amorphous alkali thio-hydroxogermanates for $x > 1$ using low-pressure sealed compacted powder pellets. Figure 10 presents an Arrhenius temperature-dependent plot of DC conductivity values for the as-prepared 2MSH + GeO_2 + $n H_2O$ reaction products (M = Na, K, Rb, and Cs), Figure 11 presents an Arrhenius temperature-dependent plot of DC conductivity values for the as-prepared 3MSH + GeO_2 + $n H_2O$ reaction products (M = Na, K, Rb, and Cs), and Figure 12 presents an Arrhenius temperature-dependent plot of DC conductivity values for the as-prepared xCsSH + GeO_2 + $n H_2O$ reaction products ($x = 1$, 2, 3 and 4). In a controlled atmosphere, the conductivity values of the cesium thio-hydroxogermanate were found to be time, temperature, and RH dependent.[21] In this work, using a low-pressure sealed assembly for the compact powder samples help minimize the effects from different thermal histories,

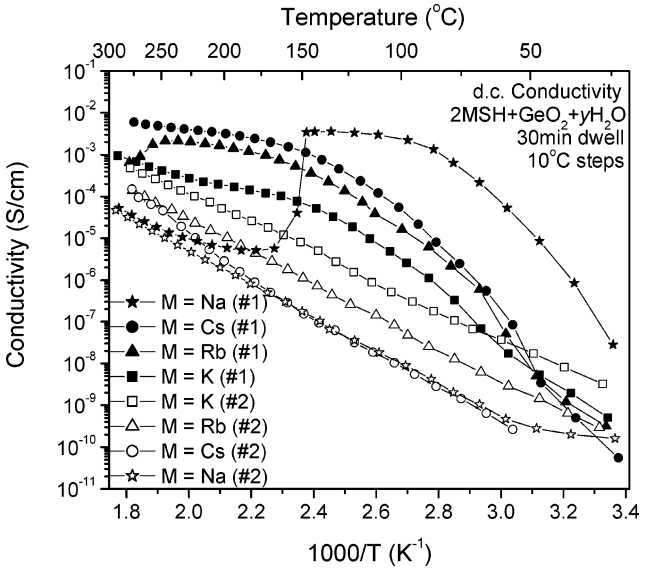

Figure 10. Arrhenius temperature-dependent plot of DC conductivity values for the as-prepared 2MSH + GeO_2 + $n H_2O$ reaction products (M = Na, K, Rb, and Cs) for the first and second heating cycles. Measurements were performed using 10 °C steps and 30-min stabilization times on compacted powder pellets sealed in a Teflon sleeve and steel electrodes.

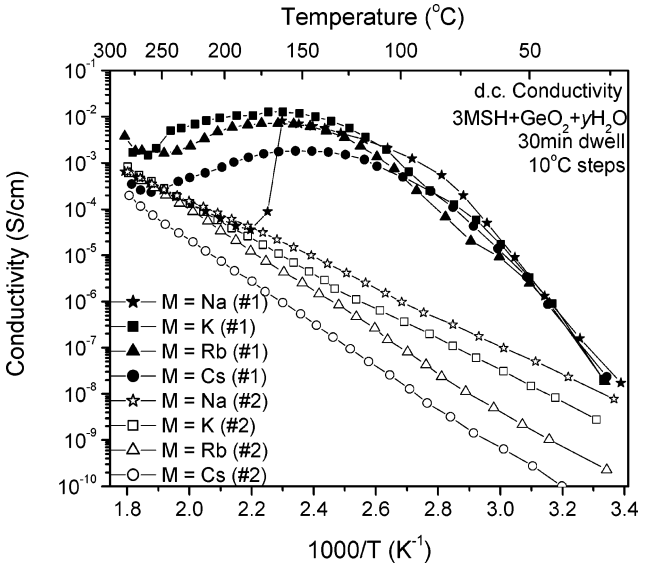

Figure 11. Arrhenius temperature-dependent plot of DC conductivity values for the as-prepared 3MSH + GeO_2 + $n H_2O$ reaction products (M = Na, K, Rb, and Cs) for the first and second heating cycles. Measurements were performed using 10 °C steps and 30-min stabilization times on compacted powder pellets sealed in a Teflon sleeve and steel electrodes.

i.e., dwell or stabilization times and temperature steps, and the sample environment more closely matched that of the hermetically sealed DSC pans. As a result, similar behavior is observed with regard to thermal stability. Specifically, the observed "drop-off" in conductivity at elevated temperatures (147−275 °C) is consistent with the sublimation behavior observed in the corresponding DSC thermograms and the inflection point temperatures observed from TGA measurements. In the series, the cesium and sodium thio-hydroxogermanates have the highest (275°C) and lowest (147°C) "drop-off" temperatures, respectively.

The ratio of proton to alkali mobility may be estimated in situ by thermally cycling the sample, i.e., AC impedance measurements from the first heating cycle represent a

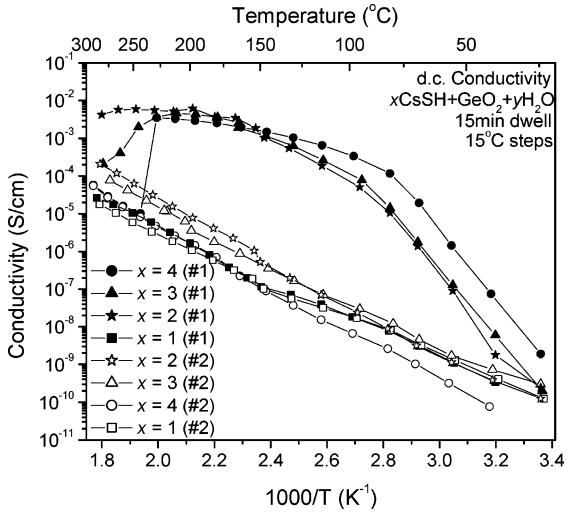

Figure 12. Arrhenius temperature-dependent plot of DC conductivity values for the as-prepared xCsSH + GeO_2 + nH$_2$O reaction products (x = 1, 2, 3 and 4) for the first and second heating cycles. Measurements were performed using 15 °C steps and 15-min stabilization times on compacted powder pellets sealed in a Teflon sleeve and steel electrodes.

combination of proton and alkali mobility, whereas these measurements from the second heating cycle predominantly represent the much lower alkali mobility of the decomposed (dehydrated) sample. Specifically, the overall magnitude of the DC conductivity values from the first heating cycle are correlated to the hydrated water (and thus alkali) content. In contrast, values from the second heating cycle are correlated to the alkali size and concentration. In the series, only the CsSH + GeO_2 + nH$_2$O reaction product had similar DC conductivity values for both the first and second heating cycles. This behavior and the absence of vibrational bands attributable to rotatory modes of hydroxide ions and water molecules (see Figure 3) indicate the importance of an extensive hydrogen-bonded network for proton conduction in these materials.

The proton conductivity of the amorphous hydrated alkali thio-hydroxogermanates appears to be mediated by both the presence of the extrinsic or hydrated water and the intrinsically bound hydroxyl groups. Generally, two competing mechanisms are expected for the proton conduction, namely, vehicle and Grotthuss or free-proton types.[32] In these materials, the conductivity is observed to increase with increasing amounts of hydrated water, which would inherently lead to a decrease in the intrinsic OH^- structural vacancies. This would indicate the primary method of proton conduction is not OH^- hopping. Additional amounts of water in these materials above the intrinsic amount of structural water (i.e., Ge−OH) may occupy well-defined OH^- "interstitial" sites within the hydrated cation shell forming $M^+\cdots OH^-$ and $Ge-S^-\cdots H^+$ hydrogen bonding or the protonation of the structural hydroxyl groups $Ge-OH^-\cdots H^+$ similarly to that proposed for NaOH·xH$_2$O.[16] This proposed behavior is in agreement with the extensive hydrogen bonded network indicated by vibrational spectroscopy and previously reported for the crystalline sodium thio-hydroxogermanates counterparts.[19,20] Thus with increasing amounts of water, a free proton mechanism is expected to dominate.

Summary and Conclusions

In summary, a new class of amorphous hydrated alkali thio-hydroxogermanates is synthesized and investigated with respect to structure and proton conductivity. The X-ray amorphous nature of these hydrated materials may be attributed to the low heating evaporation−precipitation synthesis route. The vibrational spectra indicate the presence of mixed thio-oxoanions of germanium with nonbridging sulfurs, hydrophilic alkali, and hydrated water with extensive hydrogen bonding. Further evidence of an extensive hydrogen-bonded network is noted from endothermic transitions observed between 176 and 275 °C, representing a suppression of the "boiling" point, and fast proton conductivity values (10^{-3} to 10^{-2} S/cm) were observed up to this transition. This unique class of mixed anion materials may hold potential as fast proton conductors for use in the intermediate temperature range of 100 to 300 °C.

Acknowledgment. This material is based on the work funded by the United States Department of Energy's Hydrogen Program under Cooperative Agreement No. DE-FC36-00GO1-531.

CM0488581

(32) Kreuer, K. *Chem. Mater.* **1996**, *8*, 610−641.